

# Lawrence Berkeley National Laboratory

## Recent Work

### Title

QUANTUM THEORY OF NONEQUILIBRIUM PROCESSES. II. APPLICATION TO NUCLEAR COLLISIONS

### Permalink

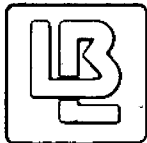
<https://escholarship.org/uc/item/4750d5td>

### Author

Danielewicz, P.

### Publication Date

1982-12-01



# Lawrence Berkeley Laboratory

UNIVERSITY OF CALIFORNIA

RECEIVED  
LAWRENCE  
BERKELEY LABORATORY

FEB 28 1983

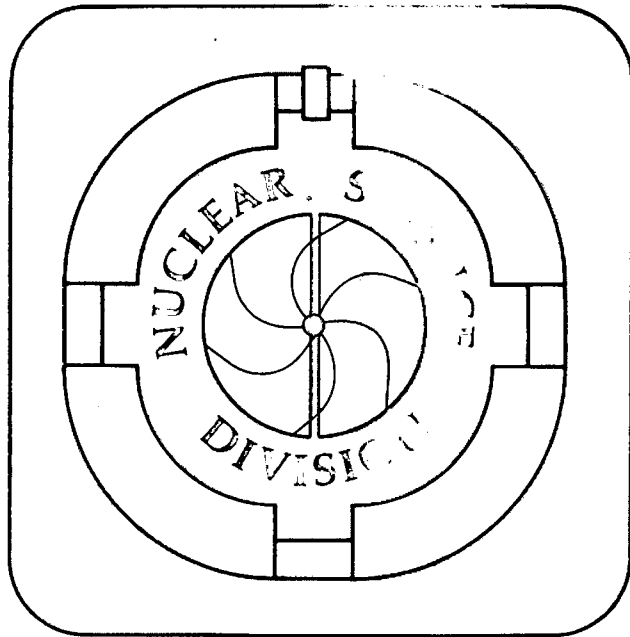
LIBRARY AND  
DOCUMENTS SECTION

Submitted to Annals of Physics

QUANTUM THEORY OF NONEQUILIBRIUM PROCESSES. II.  
APPLICATION TO NUCLEAR COLLISIONS

P. Danielewicz

December 1982



LBL-15437  
c-2

## DISCLAIMER

This document was prepared as an account of work sponsored by the United States Government. While this document is believed to contain correct information, neither the United States Government nor any agency thereof, nor the Regents of the University of California, nor any of their employees, makes any warranty, express or implied, or assumes any legal responsibility for the accuracy, completeness, or usefulness of any information, apparatus, product, or process disclosed, or represents that its use would not infringe privately owned rights. Reference herein to any specific commercial product, process, or service by its trade name, trademark, manufacturer, or otherwise, does not necessarily constitute or imply its endorsement, recommendation, or favoring by the United States Government or any agency thereof, or the Regents of the University of California. The views and opinions of authors expressed herein do not necessarily state or reflect those of the United States Government or any agency thereof or the Regents of the University of California.

Quantum Theory of Nonequilibrium Processes. II.  
Application to Nuclear Collisions\*.

P. Danielewicz<sup>†</sup>  
Nuclear Science Division  
Lawrence Berkeley Laboratory  
University of California  
Berkeley, CA 94720

ABSTRACT

In the high-energy ( $E_{\text{lab}} \gtrsim 200$  MeV/nucleon) heavy ion-collisions, the quantum uncertainty of nucleon energies, given by the collision frequency, is of the order of (50–100) MeV. At hundreds MeV/nucleon beam energies, the uncertainty is comparable with nucleon energies in the equal ion-velocity frame, indicating a quantum character of the dynamics. We examine the quantum dynamics of a collision process using nonequilibrium Green's function methods. We perform numerical calculations of collisions in an interpenetrating nuclear matter model, at the energy  $E_{\text{lab}} = 400$  MeV/nucleon. Comparison of the quantum dynamics, with the classical Markovian dynamics from the Boltzmann equation, reveals effects of the ill-defined nucleon energies in the nucleon momentum distribution. We show that the quantum dynamics proceeds twice as slow as Boltzmann dynamics, but the off-shell kinematics compensates for this somewhat.

\* This work was supported by the Director, Office of Energy Research, Division of High Energy and Nuclear Physics of the U.S. Department of Energy under Contract DE-AC03-76SF00098.

<sup>†</sup> On leave of absence from Institute of Theoretical Physics, Warsaw University, Warsaw, Poland.

## 1. Introduction

With recent availability of high-energy beams, the physics of high-energy heavy-ion collisions has undergone a rapid development. The theory of the collisions has concentrated on the explanation of basic reaction mechanisms and on the possible occurrence of exotic phenomena in the reactions (see the reviews [1,2]). In principle, a full theoretical description of the collisions would necessitate a complete relativistic quantum field theory of strong interactions. At sufficiently low density and low excitation energies of a system, it is, however, believed that nucleons may be described as structureless particles interacting via meson exchange. Below the particle production thresholds one may simplify the theory by ignoring the relativistic effects and introducing a static two-body potential for nucleons. Even within that formulation there has been so far no possibility of describing the reaction process. Because of a large number of nucleons taking part in a collision, it is not possible to evaluate an S matrix.<sup>1</sup> For low-energy heavy-ion collisions ( $E_{lab} < 10$  MeV/nucleon) one solves the equations of motion for 1-particle wave functions (1-particle density matrix) in the mean-field approximation. This approach cannot be applied at high energies, because the binary NN collisions are not suppressed by the Pauli principle and dominate the dynamics.

That situation led to the development of numerous phenomenological models for high-energy heavy-ion collisions. The idea that heavy-ion collisions can

---

<sup>1</sup> In connection with a previous paper of this series [3], we may mention that the evaluation of the S matrix for a collision corresponds through the reduction formula to an evaluation of the N-particle vacuum chronological Green's function, with N - a total number of particles.

be described classically has gained a rather common acceptance. It has been argued that the de Broglie wave length of a nucleon from an oncoming nucleus is small in comparison with a nucleon's mean free path.

In some calculations [4-9], the classical nucleons' equations of motion have been solved numerically. On the basis of a smallness of a NN interaction time, of the order of 1 fm/c, in comparison with a mean time  $\tau_{rel}$  between successive NN collisions, cascade calculations have been carried out [10-21], and the Boltzmann equation has been applied [22-24]. In the initial phase of an ion collision  $\tau_{rel} \approx 1/(n_0 \sigma v) \approx (1.7-3.5)$  fm/c, where  $n_0$  is the normal nuclear density,  $\sigma$  a total NN cross section,  $v$  a relative velocity of ions,  $E_{lab} \geq 200$  MeV/nucleon. (Because of the Pauli principle we take into account only collisions with nucleons from the opposite nucleus.) Cascade calculations and the kinetic description may be essentially considered as equivalent approaches.

A hydrodynamic description of heavy-ion collisions [25-35] relies on an assumption of a local thermodynamic equilibrium; this corresponds to a smallness of the relaxation time  $\tau_{rel}$  in comparison with the heavy-ion collision time  $\tau_{col} \lesssim 20$  fm/c.

In statistical [36,37] and thermodynamic [38-43] models one assumes that the dynamics leads to a uniform population of the available phase space.

At the beam energies per nucleon exceeding the Fermi energy, at least a doubling of the nuclear-matter density may be expected. Hypotheses have been put forward on occurrence in the dense excited matter of an anomalous nuclear state [44,45], a  $\pi$  meson condensation [46-51], or quark matter [52-54]. The calculations of these phenomena, requiring the use of a field theory, concerned static situations, and there has been no possibility of investigating exotic phenomena in dynamic situations.

Can one really describe the high-energy heavy-ion collisions classically? The mean time between successive NN collisions (the characteristic time of changes in the nucleon distribution), equal initially to  $\tau_{rel} \approx (1.7-3.5) \text{ fm}/c$ , implies uncertainties of nucleons' energies of the order of  $\hbar/\tau_{rel} \approx (55-115) \text{ MeV}$ , due to the uncertainty principle. With the diminishing role of the Pauli principle in the course of an ion collision, the mean time between successive collisions might diminish by as much as factor of two, and respectively the uncertainties could be even larger. At the beam energies  $E_{lab} < 800 \text{ MeV}/\text{nucl}$ , the nucleons will have energies less than  $200 \text{ MeV}/\text{nucl}$ , in the equal ion-velocity frame, during the whole course of the collision. This indicates that the ion-collision dynamics at these beam energies should have a quantum character, because uncertainties would be larger than or comparable with the energies of nucleons.

Even at much higher beam energies quantum effects may be expected, in cases when strong kinematical restrictions occur, e.g., in the production or absorption of particles.

In the present paper, we examine the quantum dynamics of a collision process. We perform numerical calculations of collisions in an interpenetrating nuclear matter model, at the energy  $E_{lab} = 400 \text{ MeV}/\text{nucl}$ . The quantum dynamics is confronted with a classical Markovian dynamics given by the Boltzmann equation. The calculations are the first attempt at a quantum description of a collision process at high energies. We employ the methods of nonequilibrium Green's functions, described in a previous paper of the series [3] (hereafter referred to as I).

Nonequilibrium Green's function techniques have recently received certain attention in nuclear physics. In Ref. [55] the methods have been applied to a nucleon moving in nuclear matter, radiating  $\pi$  mesons. Several authors [56-59]

have considered Green's function methods to go beyond the time-dependent Hartree-Fock approximation in the description of low-energy heavy-ion collisions.

The interpenetrating nuclear matter model, considered in the paper, has been previously applied in Refs. [50,22] (also in [60]). Randrup [22] studied the Boltzmann equation dynamics.

In calculating the nuclear-matter collisions we solve the Green's function equations of motion with self-energies. In Sect. 2 we present results for a two Fermi-spheres Hartree-Fock initial state of the nuclear system. The evolution is compared with the one given by the Boltzmann equation. Details of the calculations are contained in Appendices A and B. At initial stages of the nuclear-matter collision, the nucleon momentum distributions, resulting from the Green's function equations of motion, differ from distributions from the Boltzmann equation, reflecting ill-defined nucleon energies. The approach to equilibrium is slower in the quantum dynamics than in the Boltzmann dynamics.

In Sect. 3 we repeat the quantum calculation of the nuclear-matter collision, starting from a correlated initial state. The correlated state is prepared through the imaginary-time evolution. Details of the calculation are contained in Appx. C.

In Sect. 4, we analyse the effect of the slowing down of the quantum dynamics in comparison with the Boltzmann dynamics, observed in the calculations.

The calculations presented in the paper concern a uniform-medium problem. When solving a nonuniform problem it may be indispensable to expand the Green's functions and self-energies in some 1-particle basis. Such attempts have been presented in Refs. [56-59].



In a following paper of the series, we discuss the nonequilibrium Green's function methods for a system of fermions coupled with bosons. Results contained there should be of interest in connection with the  $\pi$ -meson condensation studies, and also the particle production in heavy-ion collisions.

## 2. Nuclear matter collisions

The model which we employ is the following. We consider spatially infinite and uniform, spin-isospin symmetric system of nucleons. At the initial moment the nucleons are confined to two separate Fermi spheres. The picture refers to the initial phase of a nuclear collision, when the nuclei have partially overlapped, but the thermalization has not yet taken place.

The radii of the Fermi spheres in the calculations have been taken equal to  $p_F = 255 \text{ MeV}/c$  (which corresponds to the normal nuclear density  $n_0 = 0.145 \text{ fm}^{-3}$ ). For numerical reasons the extent of the momentum space in the model has been limited to a sphere of a radius  $900 \text{ MeV}/c$ .

For the model system we have both solved the Green's function equations of motion, discussed in Sect. 3 of I, and the Boltzmann equation. Calculations, described in detail in Appendices A and B, have been carried out for a separation  $2 p_0$ , between the centers of the Fermi spheres, corresponding to  $E_{\text{lab}} = 400 \text{ MeV}$ . For the self-energy, in the Green's function equations of motion, the direct Born approximation has been used. Parameters of the local potential (approximation to the T-matrix) have been taken from a Born approximation fit to the differential nucleon-nucleon cross sections.

Evolutions of the nucleon momentum distribution, following from the calculations, are presented in Fig. 1. The leftmost figures represent the Boltzmann-equation evolution. The central figures represent an evolution given by the Green's function equations of motion. The evolution starts from a two Fermi-spheres Hartree-Fock initial state. The rightmost figures also represent an evolution given by the Green's function equations of motion, but one starting from a correlated initial state. The last evolution will be discussed only in the next section. In Fig. 1 the nucleon momentum distributions are seen to evolve from two separate Fermi spheres towards

equilibrium.

At an initial stage of the Boltzmann-equation evolution, a characteristic hollow shell develops in the nucleon distribution, reflecting energy and momentum conservation in binary collisions. See Fig. 1 for  $t = 0.5, 1$  fm/c, and Fig. 2 for  $t = 1, 2$  fm/c. In Fig. 2, values of the distribution functions at  $45^\circ$  and  $90^\circ$  CMS angles are depicted. According to the Boltzmann equation, a scattering of particles from two different points in the momentum space feeds a spherical shell in the momentum space. The quantum evolution gives no shell in the distribution function, which may be expected, because of ill-defined energy conservation in the interactions (see Appx. G of I) and ill-defined nucleon energies. On the basis of the equilibrium self-energy forms (Eq. (E.8) of I), one could actually consider a scattering of particles in the steady conditions of thermodynamic equilibrium. With a half-width  $\Gamma$  ( $\Gamma \sim \hbar/\tau_{rel}$ ) of initial and final states, one finds that a scattering of particles, from two different points of the momentum space, feeds a diffuse shell with a width  $2\Gamma$  in the kinetic energy of the final particle.

The approach to equilibrium is more rapid with the Boltzmann equation than with the quantum equations of motion. For an average deviation of the distribution from equilibrium  $(\int dp (f(p,t) - f_{eq}(p))^2 / \int dp f_{eq}^2(p))^{1/2}$  equal to  $1/2$ , which corresponds to  $t = 4.7$  fm/c in the Boltzmann and to  $t = 6.3$  fm/c in the quantum evolution, we get respective rates

$$\gamma := \hbar (\int dp (\partial f / \partial t)^2 / \int dp (f(p,t) - f_{eq}(p))^2)^{1/2} \text{ equal to } 73 \text{ MeV and to } 53 \text{ MeV.}$$

At the time  $t = 10$  fm/c, the nucleon distribution from the Boltzmann equation is practically at equilibrium, while the distribution from the quantum evolution still exhibits nonequilibrium features. We shall discuss the effect in some detail in Sect. 4.

To assess the validity of a hydrodynamic approach to nuclear collisions,

it is interesting to study the relaxation of the tensor  $\langle p^i p^k \rangle$  towards isotropy. The average is taken here with respect to the distribution function. In Fig. 3, an anisotropy of the tensor, given by  $(2\langle p^z{}^2 \rangle / \langle p^i{}^2 \rangle - 1)$ , is presented as a function of time. An anisotropy equal to 1/2 is achieved after 6.7 and 9.2 fm/c for the Boltzmann equation and the Green's function equations of motion, respectively.

If one goes beyond the self-energy in the Hartree-Fock approximation, in the Green's function equations of motion, then the nucleon distribution given by a Fermi sphere is not stationary. Figure 4 presents a radial profile of a single evolving Fermi sphere placed in the center of the momentum space--the calculation was performed with the same numerical code as the nuclear matter collisions. The sphere decays, occupation in the central part of the sphere drops, stabilizing at around 0.7, and the sphere acquires a tail. At a time  $t = 6$  fm/c, when we interrupt the evolution, the changes occur only in the vicinity of the Fermi momentum. In the next section we consider an evolution of the nuclear system, that starts not from the two Fermi-spheres Hartree-Fock state, but from a correlated initial state prepared through the imaginary-time evolution (Sect. 5 of I).

### 3. Dynamics for a correlated initial state

In Ref. [61] attention was paid to the fact that, if one intends to consider nucleon-nucleon collisions in nuclear collisions, then in a consistent approach to the problem one should include the collisions in the nuclear ground states. When the widths of states are finite, the occupations inside a Fermi sphere are less than unity and outside the sphere possesses a tail. At a temperature  $T = 0$  in nuclear matter, according to Eqs. (E.2a), (E.5), and (E.13) of I ( $\beta \rightarrow \infty$ ),

$$-iG^<(p, \omega) = \theta(\mu - \omega) \frac{\Gamma(p, \omega)}{(\omega - p^2/2m - \text{Re}\Sigma^+(p, \omega))^2 + (\Gamma(p, \omega)/2)^2}, \quad (3.1)$$

and the nucleon distribution

$$f(p) = \int_{-\infty}^{\mu} \frac{d\omega}{2\pi} \frac{\Gamma(p, \omega)}{(\omega - p^2/2m - \text{Re}\Sigma^+(p, \omega))^2 + (\Gamma(p, \omega)/2)^2}. \quad (3.2)$$

In the second quantum calculation of nuclear matter collision, an initial nuclear matter state was obtained from a two Fermi spheres Hartree-Fock state through the imaginary time evolution described in Sect. 5 of I. The evolution generator in the imaginary time was of the form

$$\hat{\mathcal{H}} = \hat{H} - v_0 \hat{p}^{+z} + v_0 \hat{p}^{-z}. \quad (3.3)$$

Here  $\hat{p}^{\pm z}$  are the beam-axis components of the operators of the total momentum in the forward and backward momentum space hemispheres, respectively. The Lagrange multiplier  $v_0$  has been taken equal to  $v_0 = p_0/m$ . Equation (3.3) corresponds to the replacement of 1-particle energies

$$\begin{aligned} \hat{H}^0 &= \sum_{\underline{p}\alpha} \frac{p^2}{2m} b_{\underline{p}\alpha}^{\dagger} b_{\underline{p}\alpha} \\ \Rightarrow \hat{\mathcal{H}}^0 &= \sum_{\underline{p}\alpha} \frac{p^{\perp 2} + (p^z - p_0)^2}{2m} b_{\underline{p}\alpha}^{\dagger} b_{\underline{p}\alpha} \end{aligned}$$

$$\begin{aligned}
 &= \sum_{\substack{\underline{p} \\ a\alpha}} \frac{p^{\perp 2} + (p^z + p_0)^2}{2m} \hat{b}_{\underline{p}a\alpha} \hat{b}_{\underline{p}a\alpha} \\
 &= \sum_{\underline{p}a\alpha} \frac{p^{\perp 2} + (|p^z| - p_0)^2}{2m} \hat{b}_{\underline{p}a\alpha}^\dagger \hat{b}_{\underline{p}a\alpha}
 \end{aligned} \tag{3.4}$$

Here  $\hat{b}_{\underline{p}a\alpha}$  is the annihilation operator of the state with momentum  $\underline{p}$  and respective spin and isospin projections.

The self-energy on a contour in the complex time plane has been taken in the direct Born approximation. In detail, the calculation is described in Appx. C. The nuclear matter system has been evolved in the imaginary time for 3 fm/c. In case of a single Fermi sphere, with  $\hat{\mathcal{H}} = \hat{H}$ , the chosen time of the imaginary evolution assures a reasonable stationarity of the distribution for real times.

An evolution of the nucleon distribution, for a state prepared through the imaginary evolution, is presented in Fig. 1, the rightmost figures. At an initial moment, the occupations inside the Fermi spheres are equal to about 0.8. The profiles of the distribution at 45° and 90° CMS angles are depicted in Fig. 2 (solid lines).

Early stages of distributions from the quantum and classical evolutions differ qualitatively because of the uncertainty principle. Again in the quantum evolution we obtain no shell in the momentum space. Starting from the initial state, more nucleons populate high momenta in the quantum case than in the Boltzmann equation case. These are the results of ill-defined nucleon energies and ill-defined energy conservation in the interactions, in the quantum case.

The inclusion of correlations in the initial state narrows the nucleon distributions at late stages of the evolution. The slowing down of the

quantum evolution, in comparison with the Boltzmann evolution, is now somewhat more directly visible in the nucleon distributions. Quantitatively, for an average deviation from equilibrium equal to  $1/2$  (see the previous section) at  $t = 6.9$  fm/c, we get the effective rate  $\gamma = 50$  MeV. The approach of the distribution to equilibrium turns out about 50% more rapid in the Boltzmann dynamics than in the quantum dynamics.

The time for the tensor  $\langle p^i p^k \rangle$  to achieve an anisotropy equal to  $1/2$  is now equal to  $9.9$  fm/c<sup>2</sup>, see Fig. 3.

---

<sup>2</sup> Let us mention that our finite momentum space favors quick equilibration of anisotropy, especially in the quantum dynamics.

#### 4. The slowing down of quantum dynamics

Let us discuss in some detail the slowing down of the quantum evolution.

In Fig. 5 we plot the values of the scattering-in and -out rates in the Boltzmann equation at  $90^\circ$  for  $t = 10$  fm/c. Similar values of the rates prevail throughout the momentum space during most of the evolution. The lowering of the scattering-out rate with momentum, in Fig. 5, is an effect of the Pauli principle. According to the Green's function equations of motion, the distribution function satisfies

$$\begin{aligned} \frac{\partial}{\partial t} f(\underline{p}, t) = & 2\text{Re} \left( \int_0^t dt' (-i)\Sigma^<(\underline{p}; t, t') iG^>(\underline{p}; t', t) \right. \\ & \left. - \int_0^t dt' i\Sigma^>(\underline{p}; t, t') (-i)G^<(\underline{p}; t', t) \right) . \end{aligned} \quad (4.1)$$

On the basis of (4.1) we may define auxiliary rates

$$\begin{aligned} & -i\Sigma^<(\underline{p}; t) \\ & = 2\text{Re} \left( \int_0^t dt' (-i)\Sigma^<(\underline{p}; t, t') iG^>(\underline{p}; t', t) \right) / (1 - f(\underline{p}; t)) , \end{aligned} \quad (4.2a)$$

and

$$\begin{aligned} & i\Sigma^>(\underline{p}; t) \\ & = 2\text{Re} \left( \int_0^t dt' i\Sigma^>(\underline{p}; t, t') (-i)G^<(\underline{p}; t', t) \right) / f(\underline{p}; t) , \end{aligned} \quad (4.2b)$$

and in Fig. 5 we compare the values of the rates with the values of the rates from the Boltzmann equation.<sup>3</sup> For  $\Gamma(\underline{p}; t) = i(\Sigma^> - \Sigma^<)(\underline{p}; t)$  averaged over the nucleon momentum distribution at  $t = 10$  fm/c, we get 68 MeV in the quantum calculation with the Hartree-Fock initial state and 61 MeV in the

<sup>3</sup> In the Boltzmann limit, the auxiliary rates coincide with the rates from the Boltzmann equation. In thermodynamic equilibrium, the rates are  $-i\Sigma^<(\underline{p}) = \int (d\omega/2\pi) (-i)\Sigma^<(\underline{p}, \omega) iG^>(\underline{p}, \omega) / (1 - f(\underline{p}))$ ,  $i\Sigma^>(\underline{p}) = \int (d\omega/2\pi) i\Sigma^>(\underline{p}, \omega) (-i)G^<(\underline{p}, \omega) / f(\underline{p})$ .



calculation with a correlated initial state, as compared with an average  $\Gamma$  from the Boltzmann calculation equal to 136 MeV. Average rates vary weakly throughout most of the evolutions and are seen to be about twice lower in the quantum evolutions as compared with the Boltzmann evolution. There are two reasons for the lower rates. Partially the lowering comes from the decay of the Green's functions as functions of difference of time arguments. We plot the functions' moduli for several momenta in Fig. 6. Straight lines drawn in the figure correspond to exponential decay rates  $\Gamma(p;t)/2$ . An exponential decay  $|G^{\lambda}(p;t,t')| = |G^{\lambda}(p)| \times \exp(-\frac{1}{2}\Gamma(p,\omega_p)|t-t'|)$  is found in thermal equilibrium (Appx. E of I), when one ignores the frequency dependence of self-energies in the spectral function, Eq. (E.5) of I, and in the expressions for  $G^{\lambda}$ , Eq. (E.2) of I, one replaces the occupation function  $f$  with its value at  $\omega = \omega_p$ . Coupling to macroscopic variations in the system is particularly evident for a momentum inside the Fermi sphere, Fig. 6d. The decay of the Green's functions restricts the time integration ranges in Eq. (4.1) (see Eqs. (G.5) and (G.6) of I) and reduces the integrals. We may consider that the decay of the Green's functions in the integrals accounts for an overlapping of the interaction zones in the medium, which is due to finite interaction times. By considering the equilibrium functions in the frequency representation, it may be seen that finite widths of the states in the self-energy integrals induce high-momentum transfers in the scattering, hence the cross section drops. Apart from the mere decay of the Green's functions, there is another effect that, as the numerical investigations show, is responsible for most of the drop of the rates. This is a rather different oscillatory behavior of the functions  $G^<$  and  $G^>$  for a given momentum, as functions of the time argument difference. In fact, from Eqs. (E.2), (E.5), and (E.13) of I, a necessary existence of a frequency gap, between the functions  $G^<$  and  $G^>$ , follows for  $\beta\Gamma \sim 1$ , with the particle frequencies

lying below hole frequencies. (For reference, in the Boltzmann calculation we have  $T = \beta^{-1} \approx 80$  MeV.) In the low-density limit, for small  $\beta\Gamma$ , the gap can be expected to be of the order of  $\beta\Gamma^2$ . With  $\Gamma \approx n\sigma v$ , we have  $\beta\Gamma^2 \sim 1/(m\lambda^2)$ , where  $\lambda = 1/(n\sigma)$  stands for the mean free path, and the effect seems to be related to the energy spacing of levels in a finite spatial region.

Despite a factor of two difference in the magnitudes of the scattering-out and -in rates in the Boltzmann and quantum evolutions, the actual approach to equilibrium of the distribution from the Boltzmann equation is not that much more rapid (as is indicated by the values of effective rates quoted earlier). This is due to the following: On the approach to equilibrium there are two regions in the momentum space with excessive particle density, around the two original Fermi spheres. In the Boltzmann dynamics, because of momentum and energy conservation in binary interactions, the feeding of the momentum space from scattering of particles from one excessive region is basically restricted to the same region. By contrast, in the quantum dynamics the feeding from such scattering is in principle smeared over the whole momentum space.

To demonstrate the effect of the slowing down of the quantum evolution, we have repeated the calculations for the potential in the equations multiplied by a constant that has been varied from one set of calculations to the other. In the Boltzmann equation the operation amounts to the scaling of time variable and values of rates (uniform medium). In Fig. 7 we plot the values of the effective rates  $\gamma$  in the quantum evolutions vs effective rate  $\gamma$  in the Boltzmann evolution, at a fixed average deviation from equilibrium, when the multiplication constant is varied. Figure 8 displays values of  $\Gamma(\underline{p};t)$  averaged over particle momentum distribution close to equilibrium vs average  $\Gamma$  from the Boltzmann equation. Note the saturation of the quantum rate!

## 5. Final remarks

We have applied the nonequilibrium Green's function methods to study the quantum dynamics of a heavy-ion collision process. In heavy-ion collisions at hundreds MeV/nucleon beam energies, the quantum uncertainty of nucleon energies, of the order of NN collision rate, is comparable with nucleon energies. For that reason, inappropriate in describing the collisions are the classical equations of motion [4-9], cascade calculations [10-21], or the Boltzmann equation [22-24], and indispensable is the quantum description. The quantum description may be even necessary at much higher beam energies, for processes with strong kinematical restrictions.

Let us mention that, at beam energies lower than the Fermi energy, the collision rate drops because of the Pauli principle. Use of the self-consistent equations, supplied with a Boltzmann-type collision-term for states close to the Fermi surface, should be justified at sufficiently low energies.

We have carried numerical calculations of collisions in an interpenetrating nuclear-matter model. We have compared the Boltzmann equation dynamics with a dynamics given by the Green's function equations of motion. The quantum calculations have been performed for two types of an initial state: the Hartree-Fock state, and the correlated state. To the author's knowledge, the calculations of the present paper are the first attempt at a quantum description of the collision process. The quantum dynamics differs qualitatively from the Boltzmann dynamics. The nucleon momentum distributions evolve through different shapes, in effect of the ill-defined nucleon energies and the ill-defined energy-conservation in the interactions in the quantum case. The quantum dynamics proceeds at a slower rate, which may be traced to the energy spacing of levels in a spatial region of a dimension of the mean free-path. When artificially increasing

cross-sections in the Boltzmann-equation dynamics, the rates from the corresponding quantum dynamics exhibit a saturating behaviour.

It should be noted that the time for achieving an isotropy of the nucleon momentum distribution occurs to be unfavourably large regarding the possibility of a hydrodynamic description [25-35] of heavy-ion collision.

In real nuclear collisions, phenomena observed in nuclear-matter collisions will be modified by finite particle-number effects. The collisions will be affected by the uncertainty principle in space and momentum. Of a special interest in the collisions is the problem of particles going on-shell during the expansion of the system into vacuum.

#### Acknowledgment

Discussions with M. Gyulassy have proven very useful in development of this paper of the series, and are gratefully acknowledged.

Appendices. Calculations of nuclear-matter collisions

For the outline of the formalism see I [3].

A. Green's function equations of motion

Because of the homogeneity of the system we employ the momentum representation for the Green's functions and self-energies. If we adopt an interaction independent of the spin and isospin, then in the spin-isospin symmetric system the functions will be diagonal in the spin and isospin indices

$$F_{\alpha\beta}^{ab}(\underline{p};t,t') = \delta_{ab} \delta_{\alpha\beta} F(\underline{p};t,t') .$$

From Eqs. (3.1) and (3.2) of I we have for  $t \neq t'$  on the contour

$$\left(i\frac{\partial}{\partial t} - \frac{p^2}{2m}\right)G(\underline{p};t,t') = \int_{t_0}^t dt'' \Sigma(\underline{p};t,t'')G(\underline{p};t'',t') , \quad (A.1)$$

$$\left(-i\frac{\partial}{\partial t'} - \frac{p^2}{2m}\right)G(\underline{p};t,t') = \int_{t_0}^t dt'' G(\underline{p};t',t'')\Sigma(\underline{p};t'',t') , \quad (A.2)$$

and from (2.12) of I

$$iG^>(\underline{p};t,t) = 1 - (-i)G^<(\underline{p};t,t) . \quad (A.3)$$

The nucleon momentum-distribution is given by  $f(\underline{p},t) = -iG^<(\underline{p};t,t)$ .

The self-energy in the calculations has been taken in the direct Born approximation

$$\begin{aligned} \Sigma^>(\underline{p};t,t') &= 4 \int \frac{d\underline{p}_1}{(2\pi)^3} \int \frac{d\underline{p}'}{(2\pi)^3} (V(\underline{p}'-\underline{p}))^2 G^>(\underline{p}_1;t',t) G^>(\underline{p}';t,t') \\ &\quad \times G^>(\underline{p}+\underline{p}_1-\underline{p}';t,t') . \end{aligned} \quad (A.4)$$

The factor 4 comes from the summation over spin and isospin indices. The potential (approximation to the T-matrix) had to be taken local - depending only on the momentum transfer - in order that the numerical calculations could be carried. The parameters of the potential of a gaussian form,

$$V(\underline{p}) = \pi^{3/2} n^3 V_0 \exp\left(-\frac{1}{4} n^2 p^2\right) , \quad (\text{A.5})$$

have been fitted, within the Born approximation, to the spin-isospin averaged differential nucleon-nucleon cross-sections, in the energy range  $E_{\text{lab}} = (0-500)$  MeV. The parameters of the potential were the following:  $n = 0.57$  fm,  $|V_0| = 453$  MeV. We did not introduce the Hartree-Fock energy which could influence the evolution of the distribution function only indirectly. (In a homogenous system, for a local interaction, the direct term of the Hartree-Fock energy may be besides ruled out from the equations of motion.)

In the momentum space, Fig. 9, a mesh has been taken with an interval between the points 54 MeV/c. Symmetries of the system have been exploited: the axial symmetry with respect to the collision axis, and the reflection symmetry with respect to a plane perpendicular to the collision axis. The initial Green's functions

$$-iG^<(\underline{p}; t_0, t_0) = \begin{cases} 1 & \underline{p} \text{ inside the Fermi spheres} \\ 0 & \underline{p} \text{ outside the Fermi spheres.} \end{cases} \quad (\text{A.6})$$

Differential equations of motion (A.1) and (A.2) have been solved with a predictor - central point-slope method, and a corrector - trapezoidal method, and in solving the factor  $\exp(-i(p^2/2m)(t-t'))$  has been excluded from the Greens functions. The hermiticity of the Green's functions

$$iG^>(\underline{p}; t', t) = [iG^<(\underline{p}; t, t')]^* , \quad (\text{A.7})$$

and the relation (A.3) have been exploited. The step in time was equal to 0.5 fm/c. The time integrations at the r.h.s. of Eqs. (A.1) and (A.2) have been evaluated with a trapezoidal method. The momentum integrals in the self-energies (A.4) have been evaluated through subsequent Fourier transformations. The application of that method was critical for the possibility of accomplishing numerical calculations of nuclear-matter collisions.

Stability of the solution against the variation of the time step has been tested. It was found that the chosen size of the momentum space affects the solution to a certain extent.

During the calculated evolution (0-10) fm/c, the number of nucleons per unit volume was conserved with an accuracy of 0.2%, and the energy with an accuracy of 1%.

Within the first 2 fm/c of the evolution of the nuclear-matter system, roughly 30 MeV/nucleon of the kinetic energy is released. Later on the kinetic energy remains essentially constant.

In the additional nuclear-matter collision calculations, when the potential was multiplied by some constant, the time step was reduced to 0.25 fm/c for the constant equal to or exceeding  $\sqrt{2}$ .

#### B. Boltzmann equation

The Boltzmann equation for the distribution function  $f$  is of the form

$$\frac{\partial f(\mathbf{p}, t)}{\partial t} = 4 \int \frac{d\mathbf{p}_1}{(2\pi)^3} d\Omega' (|\mathbf{p}-\mathbf{p}_1|/m)(m^2/16\pi^2)(V(\mathbf{p}'-\mathbf{p}))^2 \\ [(1-f(\mathbf{p}, t))(1-f(\mathbf{p}_1, t))f(\mathbf{p}', t)(f(\mathbf{p}'_1, t)) \\ - f(\mathbf{p}, t)f(\mathbf{p}_1, t)(1-f(\mathbf{p}', t))(1-f(\mathbf{p}'_1, t))] . \quad (\text{B.1})$$

The integration  $\int d\Omega'$ , over the solid angle determining the orientation of the relative momentum, and the factors next to the potential, come from integration of the  $\delta$  functions of energy and momentum conservation in the collision integral.

In the momentum space a mesh has been taken, such as in the quantum case. The differential equation in time (B.1) has been solved using second-order methods as in the quantum case. The integral at the r.h.s. of (B.1) has been evaluated with a Monte-Carlo method. The method was devised so

that it would treat possibly equally various areas of the momentum space, and give possibly small fluctuations in the distributions. The number of nucleons per unit volume was conserved with an accuracy of 2%, and the energy with an accuracy of 4%. To the results presented in Figs. 1 and 2 certain smoothing has been applied. The smoothing was only effective in the initial stages of the evolution.

C. Green's function equations of motion on the contour in the imaginary time plane

From Eq. (6.20) of I, with Eqs. (6.25) and (6.26) of I, we have for  $t \neq t'$  on the contour

$$(i\frac{\partial}{\partial t} - \omega_{\tilde{p}}^0(t))G(\tilde{p};t,t') = \int_{t_0+i\tau_0}^{t_0-i\tau_0} dt'' \Sigma(\tilde{p};t,t'')G(\tilde{p};t'',t') \quad , \quad (C.1)$$

$$(-i\frac{\partial}{\partial t'} - \omega_{\tilde{p}}^0(t'))G(\tilde{p};t,t') = \int_{t_0+i\tau_0}^{t_0-i\tau_0} dt'' G(\tilde{p};t,t'')\Sigma(\tilde{p};t'',t') \quad , \quad (C.2)$$

where

$$\omega_{\tilde{p}}^0(t) = \begin{cases} \frac{p^2 + (|p^Z| - p_0)^2}{2m} & t \text{ at the imaginary part of the contour,} \\ \frac{p^2}{2m} & t \text{ real.} \end{cases} \quad (C.3)$$

From the field-operator commutation rules, there follows a relation (A.3) for the Green's functions on a contour, Eq. (6.17) of I.

The self-energy on a complex contour has been taken in the direct Born approximation (A.4). The boundary Green's function values for the imaginary evolution are

$$-iG^<(\tilde{p};t_0-i\tau_0,t_0-i\tau_0) = -iG^<(\tilde{p};t_0+i\tau_0,t_0+i\tau_0)$$



$$= \begin{cases} 1 & \rho \text{ inside the Fermi spheres,} \\ 0 & \rho \text{ outside the Fermi spheres.} \end{cases} \quad (\text{C.4})$$

First in the calculation, in a self consistent manner, the evolution equations on the imaginary part of the contour, Fig. 7 of I, have been solved. With real boundary values for functions  $iG^{\lambda}$  ((C.4) and (A.3)), the functions  $iG^{\lambda}$  and  $i\Sigma^{\lambda}$  are real on the imaginary part of contour. The time of the imaginary evolution  $\tau_0$  was taken equal to 3 fm/c. Both for the imaginary and real times the time step was equal to 0.5 fm/c. The number of nucleons, and for the real times energy, were conserved in the calculation respectively with accuracies of 0.2% and 2.5%.

The kinetic energy, larger by about 10 MeV/nucleon than in the Boltzmann dynamics, remains essentially constant throughout the evolution.

In the additional nuclear-matter collision calculations, the time step was eventually reduced to 0.25 fm/c, as in the calculations with a non-correlated initial state. The time of imaginary evolution  $\tau_0$  has been kept constant.

## References

1. J. R. Nix, Prog. Part. Nucl. Phys. 2 (1979), 237.
2. M. Gyulassy, "Relativistic Nuclear Collisions: Theory.", Lecture Notes 1980 INS Kikuchi Summer School on Nuclear Physics at High Energies, p. 157, Fuji-Yoshida, Japan, July 1-4, 1980; S. Nagamija and M. Gyulassy, "High-Energy Nuclear Collisions", Lawrence Berkeley Laboratory Report LBL-14035 (1982).
3. P. Danielewicz, "Quantum Theory of Nonequilibrium Processes. I", Lawrence Berkeley Laboratory Report LBL-15436.
4. A. R. Bodmer and C. N. Panos, Phys. Rev. C15 (1977), 1342; Nucl. Phys. A356 (1981), 517.
5. A. R. Bodmer, C. N. Panos, and A.D. MacKellar, Phys. Rev. C22 (1980), 1025.
6. L. Wilets, E. M. Henley, M. Kraft, and A. D. MacKellar, Nucl. Phys. A282 (1977), 361.
7. L. Wilets, Y. Yariv, and R. Chestnut, Nucl. Phys. A301 (1978), 359.
8. D. J. E. Callaway, L. Wilets, and Y. Yariv, Nucl. Phys. A327 (1979), 250.
9. Y. Kitazoe, M. Sano, and K. Y. Yamamoto, J. Phys. Soc. Jpn. Suppl. 44 (1978), 386.

10. J. P. Bondorf, P. J. Siemens, S. Garpman, and E. C. Halbert, *Z. Phys.* 279 (1976), 385.
11. J. P. Bondorf, H. T. Feldmeier, S. Garpman, and E. C. Halbert, *Phys. Lett.* 65B (1976), 217.
12. R. K. Smith and M. Danos, *Proc. Topical Conf. on Heavy Ion Collisions* p. 363, Fall Creek Falls, ORNL Report Conf-770602, 1977.
13. K. K. Gudima and V. D. Toneev, *Yad. Fiz.* 27 (1978), 658 [*Sov. J. Nucl. Phys.* 27 (1978), 351]; Dubna Report E2-12644 (1979).
14. K. K. Gudima, H. Iwe, and V. D. Toneev, *J. Phys.* G5 (1979), 229.
15. H. Iwe, *J. Phys.* G5 (1979), 1405.
16. J. D. Stevenson, *Phys. Rev. Lett.* 41 (1978), 1702.
17. W. Jaishi, H. Kuhlmann, and C. C. Noack, *Proc. Symp. on Relativistic Heavy Ion Research*, p. 365, Darmstadt, GSI Report P-5-78, 1978.
18. Y. Yariv and Z. Fraenkel, *Phys. Rev.* C20 (1979), 2227; C24 (1981), 488.
19. J. Cugnon, *Phys. Rev.* C22 (1980), 1885.
20. J. Cugnon, T. Mizutami, and J. Vandermeulen, *Lett. Nuovo Cimento* 28 (1980), 55; *Nucl. Phys.* A352 (1981), 505.

21. E. C. Halbert, Phys. Rev. C23 (1981), 295.
22. J. Randrup, Nucl. Phys. A314 (1979), 429.
23. R. Malfliet and Y. Karant, Phys. Lett. 86B (1979), 251; R. Malfliet, Phys. Rev. Lett. 44 (1980), 864.
24. R. Malfliet, Nucl. Phys. A363 (1981), 429, 456.
25. A. A. Amsden, F. H. Harlow, and J. R. Nix, Phys. Rev. C15 (1977), 2059.
26. A. A. Amsden, A. S. Goldhaber, F. H. Harlow, and J. R. Nix, Phys. Rev. C17 (1978), 2080.
27. W. Greiner et al. , Z. Physik A273 (1975), 359.
28. H. Stöcker, J. A. Maruhn, and W. Greiner, Phys. Lett. 81B (1979), 303; Z. Physik A290 (1979), 297; A293 (1979), 173.
29. C. Y. Wong, J. A. Maruhn, and T. A. Welton, Nucl. Phys. A253 (1975), 469; Phys. Lett. 66B (1977), 19.
30. H. H. K. Tang and C. Y. Wong, Phys. Rev. C21 (1980), 1846.
31. M. I. Sobel, P. J. Siemens, J. P. Bondorf, and H. A. Bethe, Nucl. Phys. A251 (1975), 502.

32. Y. Kitazoe, K. Matsuoka, and M. Sano, *Progr. Theor. Phys.* 56 (1976), 860.
33. P. Danielewicz, *Nucl. Phys.* A314 (1979), 465.
34. L. P. Csernai and H. W. Barz, *Z. Physik* A296 (1980), 173.
35. L. P. Csernai and B. Lukács, "Viscous Hydrodynamical Model for Relativistic Heavy Ion Reactions", Central Research Institute for Physics Report KFKI-79-58, Budapest, 1979.
36. J. Knoll, *Phys. Rev.* C20 (1979), 773.
37. J. Knoll, *Nucl. Phys.* A343 (1980), 511.
38. G. D. Westfall et al., *Phys. Rev. Lett.* 37 (1976), 1202.
39. W. D. Myers, *Nucl. Phys.* A296 (1978), 177.
40. J. Gosset, J. I. Kapusta, and G. D. Westfall, *Phys. Rev.* C18 (1978), 844.
41. S. Das Gupta and C. S. Lam, *Phys. Rev.* C20 (1979), 1192.
42. P. Danielewicz and J. M. Namysłowski, *Acta Phys. Pol.* B12 (1981), 695.
43. S. Das Gupta and A. Z. Mekijan, *Phys. Reports* 72 (1981), 131.

44. T. D. Lee, Rev. Mod. Phys. 47 (1975), 267.
45. J. Boguta, "Can Nuclear Interactions Be Long Ranged?", Lawrence Berkeley Laboratory Report LBL-14753, 1982.
46. A. B. Migdal, "Fermiony i bozony v sil'nykh pol'yakh", Nauka, Moscow, 1978.
47. A. B. Migdal, Rev. Mod. Phys. 50 (1978), 107.
48. W. Weise and G. E. Brown, Phys. Reports 27C (1976), 1.
49. V. Ruck, M. Gyulassy, and W. Greiner, Z. Phys. A277 (1976), 391.
50. M. Gyulassy and W. Greiner, Ann. Phys. (N.Y.) 109 (1977), 391;  
M. Gyulassy, Proc. Topical Conf. on Heavy Ion Collisions, p. 457,  
Fall Creek Falls, ORNL Report Conf-770602, 1977.
51. G. G. Bunatyan, Yad. Fiz. 31 (1980), 1186 [Sov. J. Nucl. Phys. 31  
(1980), 613].
52. S. A. Chin, Phys. Lett. 78B (1978), 552.
53. J. I. Kapusta, Nucl. Phys. B148 (1979), 461.
54. J. Kuti, B. Lukács, J. Polonyi, and K. Szlachanyi, Phys. Lett. 95B  
(1980), 75.

55. W. Bloss, D. Hone, and D. J. Scalpino, Nucl. Phys. A314 (1979), 346.
56. C. Y. Wong and H. H. K. Tang, Phys. Rev. Lett. 16 (1978), 1070.
57. C. Y. Wong and H. H. K. Tang, Phys. Rev. C20 (1979), 1419.
58. H. Orland and R. Schaeffer, Saclay Report DPh-T/78/41, 1978.
59. C. M. Shakin and M. S. Weiss, Lawrence Livermore Laboratory Report UCRL-80500, 1977.
60. P. Danielewicz, Abstracts of Contributed Papers, Int. Conf. on Extreme States in Nuclear Systems, p. 10, Rossendorf Report ZfK 404, 1980.
61. H. Orland and R. Schaeffer, Nucl. Phys. A299 (1978), 442.

Figure Captions

Fig. 1. Contour plots of the evolving nucleon momentum distribution  $f(p^{\perp}, p^z, t)$ . Leftmost figures - Boltzmann equation evolution; central figures - Green's function equation of motion evolution for a two Fermi-spheres Hartree-Fock initial state; rightmost figures - evolution for a correlated initial state. Horizontal axes are the collision axes. The momentum space is restricted to 900 MeV/c as shown by the outer circles.

Fig. 2. Nucleon momentum distributions at  $45^\circ$  and  $90^\circ$  CMS-angles. Short-dashed lines - distributions from the Boltzmann equation. Long-dashed lines - distributions from the Green's function equations with a Hartree-Fock initial state. Solid lines - distributions from equations with a correlated initial state.

Fig. 3. Evolution of the momentum distribution anisotropy. Short-dashed line corresponds to the Boltzmann equation, long-dashed line to the Green's function equation of motion and the Hartree-Fock initial state, and solid line to the correlated initial state. The dashed horizontal line at 0.5 is a guide to the eye representing  $\langle p^{z2} \rangle = 1.5 \times (\langle p^{\perp 2} \rangle / 2)$ .

Fig. 4. Radial profile of a single evolving Fermi sphere. An initial state of the evolution was a Hartree-Fock state.

Fig. 5. Scattering-out  $i\mathcal{Z}^>(\underline{p}, \omega_p^0; t)$  and -in  $(-i)\mathcal{Z}^<(\underline{p}, \omega_p^0; t)$  rates from the Boltzmann equation at  $90^\circ$  CMS angle (short-



dashed lines). The rates from the Boltzmann equation are depicted together with the auxiliary rates from the Green's function equations (see text), for a Hartree-Fock initial state - long-dashed lines and for a correlated initial state - solid lines.

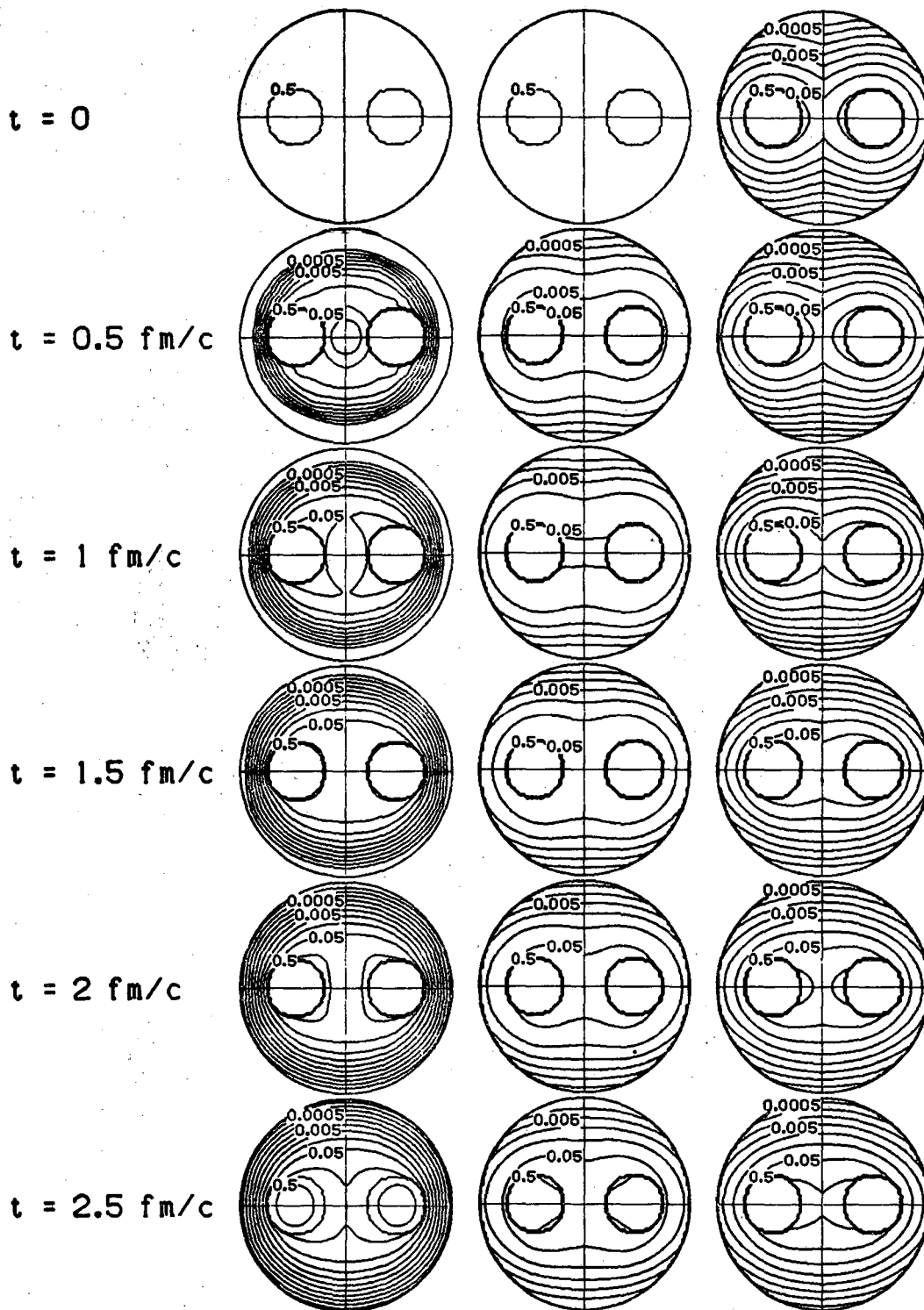
Fig. 6. Green's function moduli  $|G^2(\underline{p};t,t')|$  as functions of  $(t - t')$ , for several momenta and  $t = 10$  fm/c. Thin straight lines correspond to exponential decay rates  $\Gamma(\underline{p};t)/2$  (see text).

Fig. 7. Effective rates  $\gamma = \hbar(\int d\underline{p} (\partial f(\underline{p},t)/\partial t)^2 / \int d\underline{p} (f(\underline{p},t) - f_{eq}(\underline{p}))^2)^{1/2}$  from quantum evolutions plotted vs  $\gamma$  from Boltzmann evolution, for a fixed average deviation from equilibrium  $(\int d\underline{p} (f(\underline{p},t) - f_{eq}(\underline{p}))^2 / \int d\underline{p} f_{eq}^2(\underline{p}))^{1/2} = 1/2$ , when the multiplication constant in the potential is varied. Long-dashed line corresponds to a Hartree-Fock initial state, solid line - to correlated initial states. Short-dashed line  $\gamma = \gamma_{Boltzmann}$  serves as a guide to the eye. The arrow locates the values corresponding to the multiplication constant in the potential equal to 1.

Fig. 8. Rates  $\Gamma(\underline{p};t)$  from quantum evolutions, averaged over momentum distributions close to equilibrium, plotted vs averaged  $\Gamma(\underline{p},\omega_p^0;t)$  from Boltzmann equation, when the multiplication constant in the potential is varied. Long-dashed line corresponds to a Hartree-Fock initial state, solid -

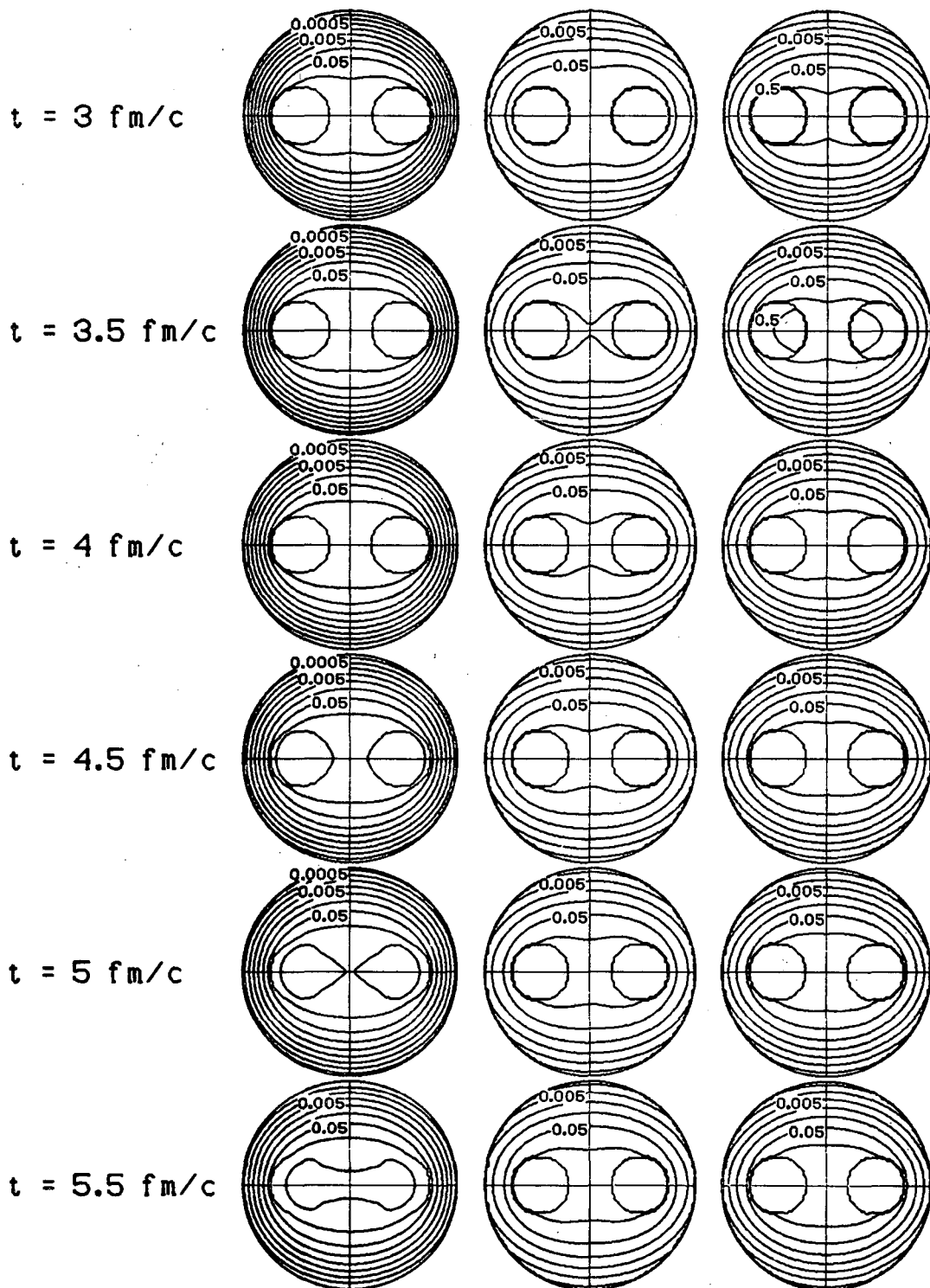
to correlated initial states. Short-dashed line  $\langle \Gamma \rangle =$   
 $\langle \Gamma \rangle_{\text{Boltzmann}}$  serves as a guide to the eye. The arrow locates  
the values corresponding to the multiplication constant in the  
potential equal to 1.

Fig. 9. Mesh in the momentum space for the numerical calculations.



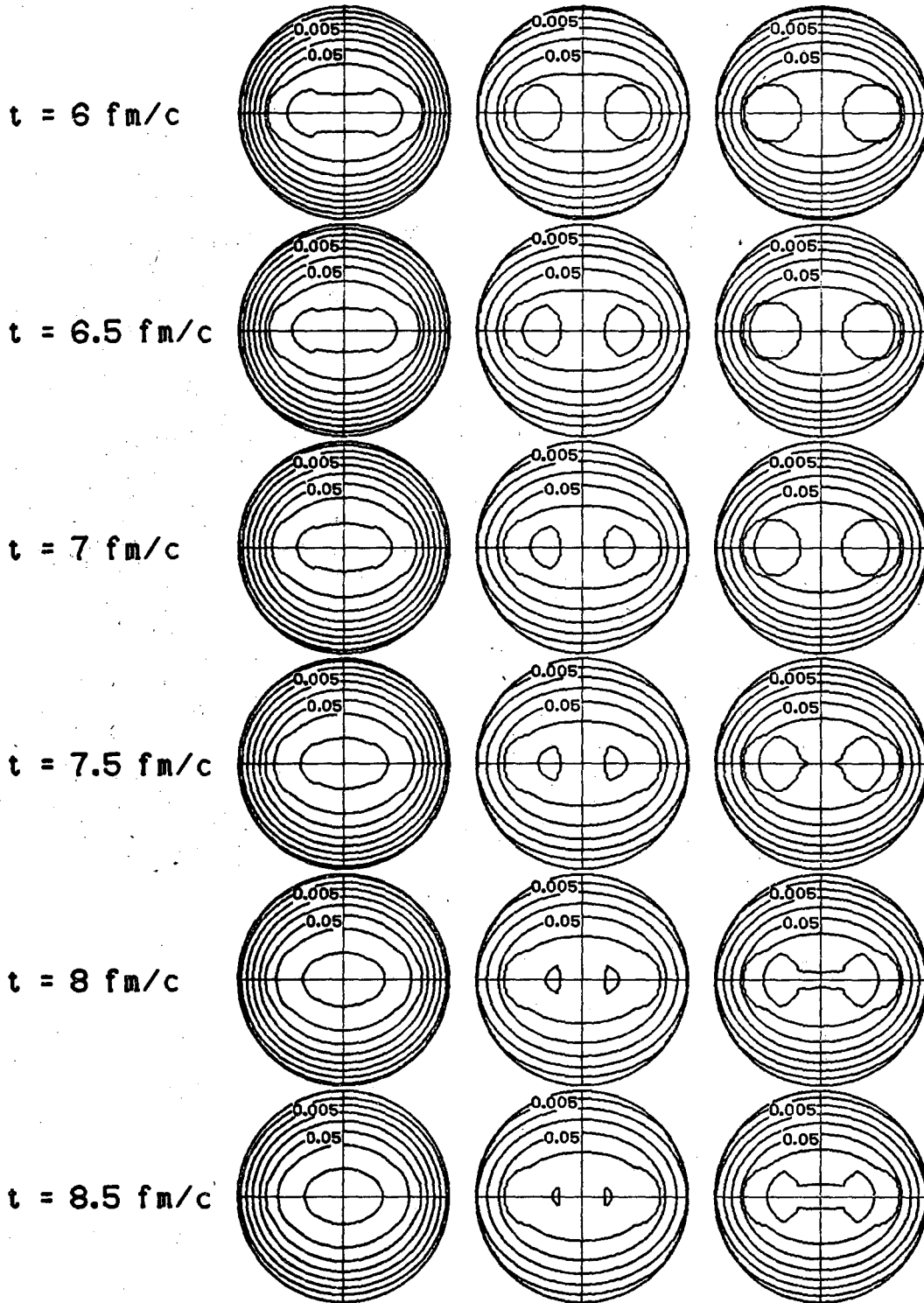
XBL 8212-12083

Fig. 1a



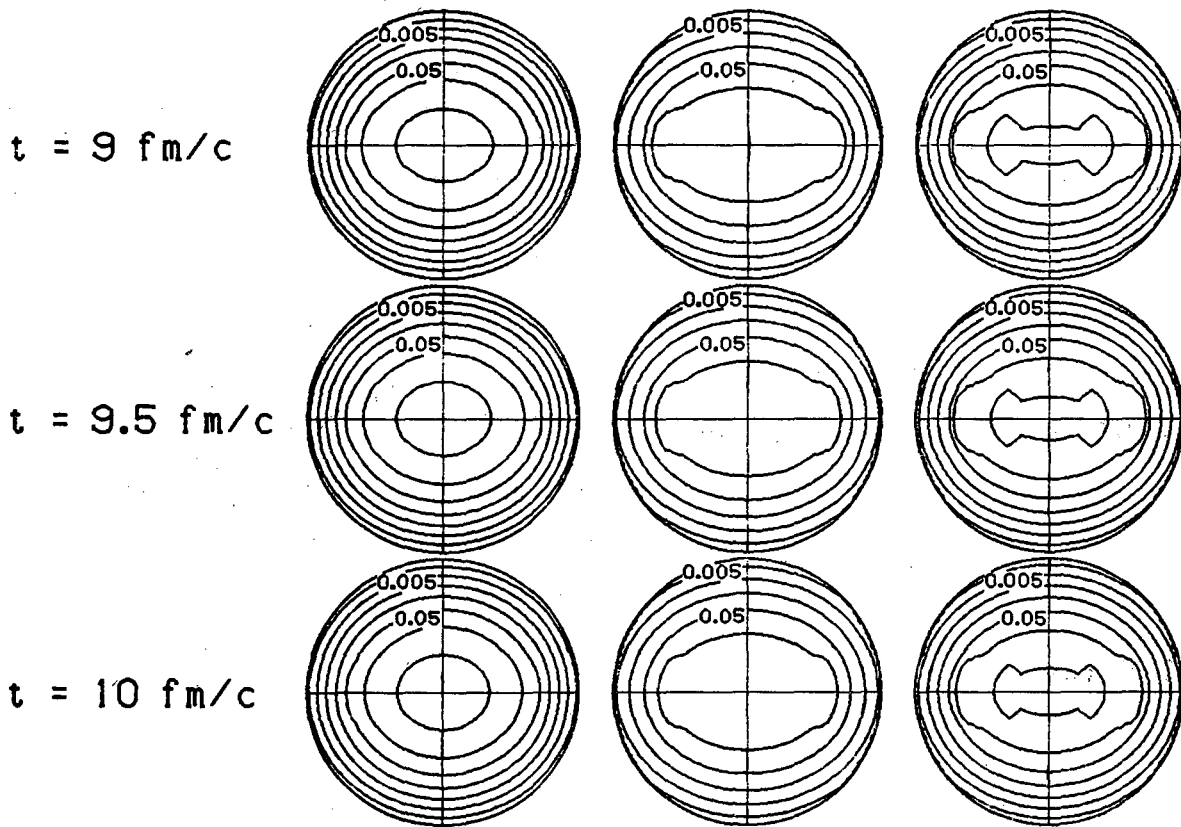
XBL 8212-12084

Fig. 1b



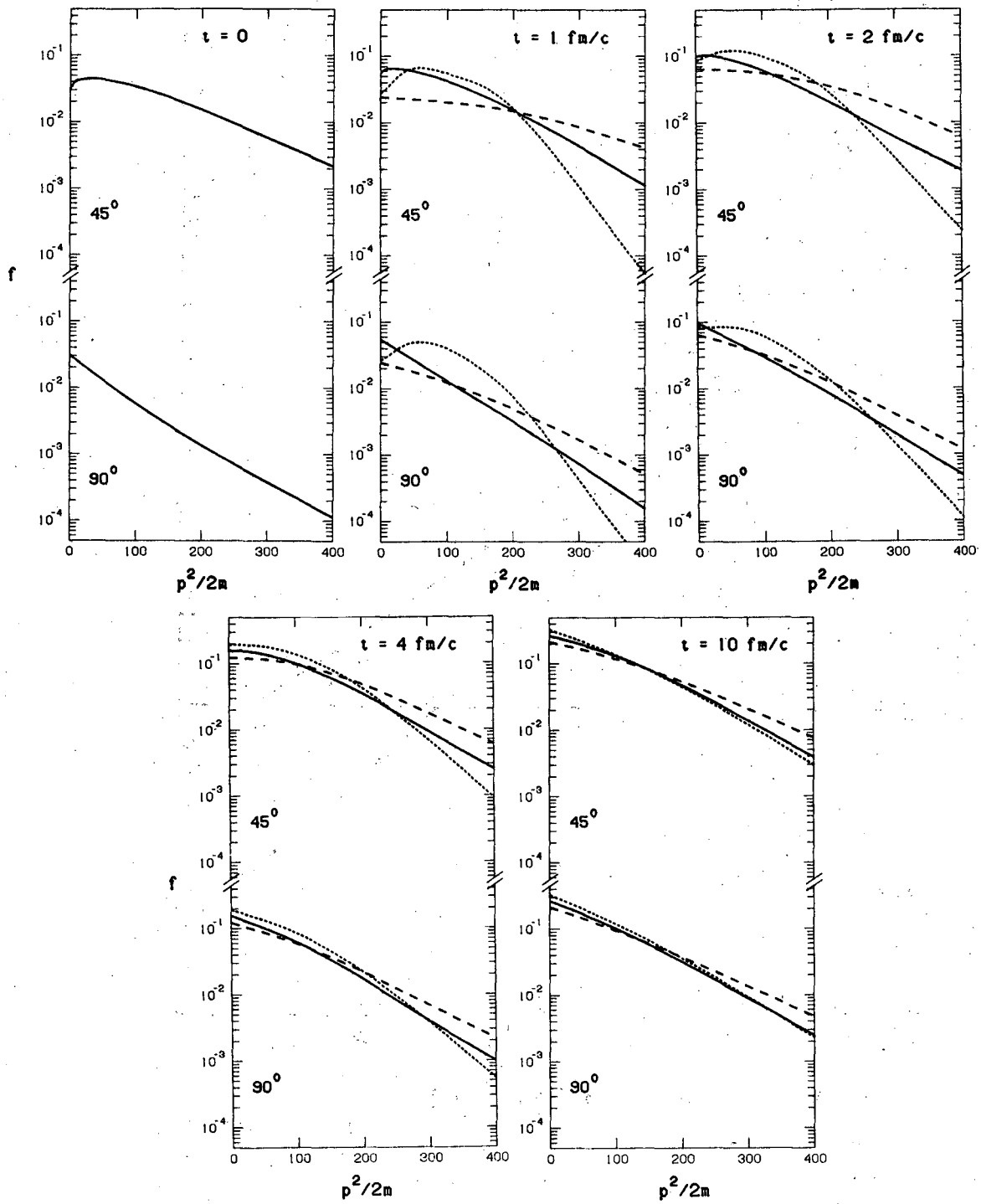
XBL 8212-12085

Fig. 1c



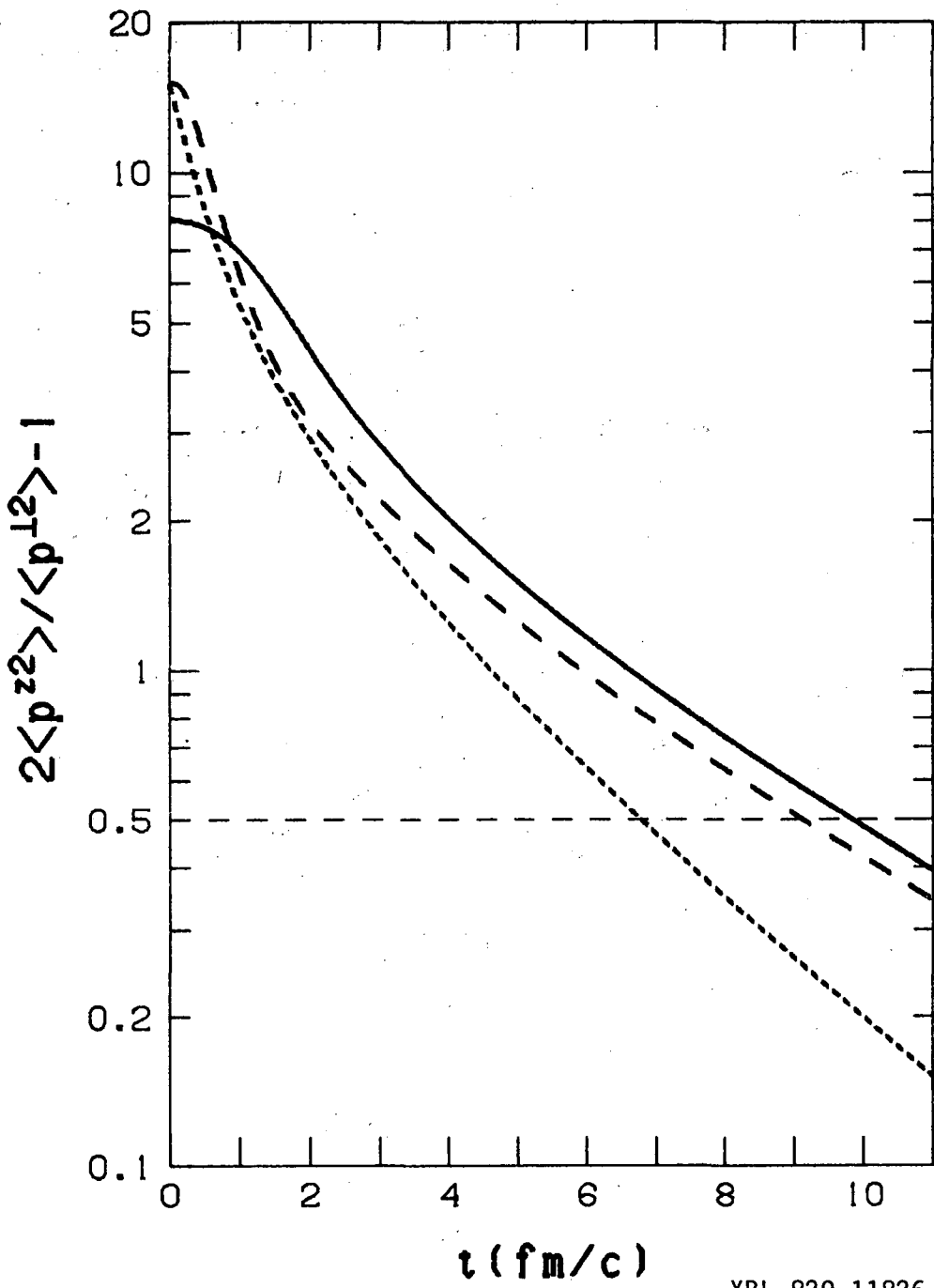
XBL 8212-12086

Fig. 1d



XBL 829-11825

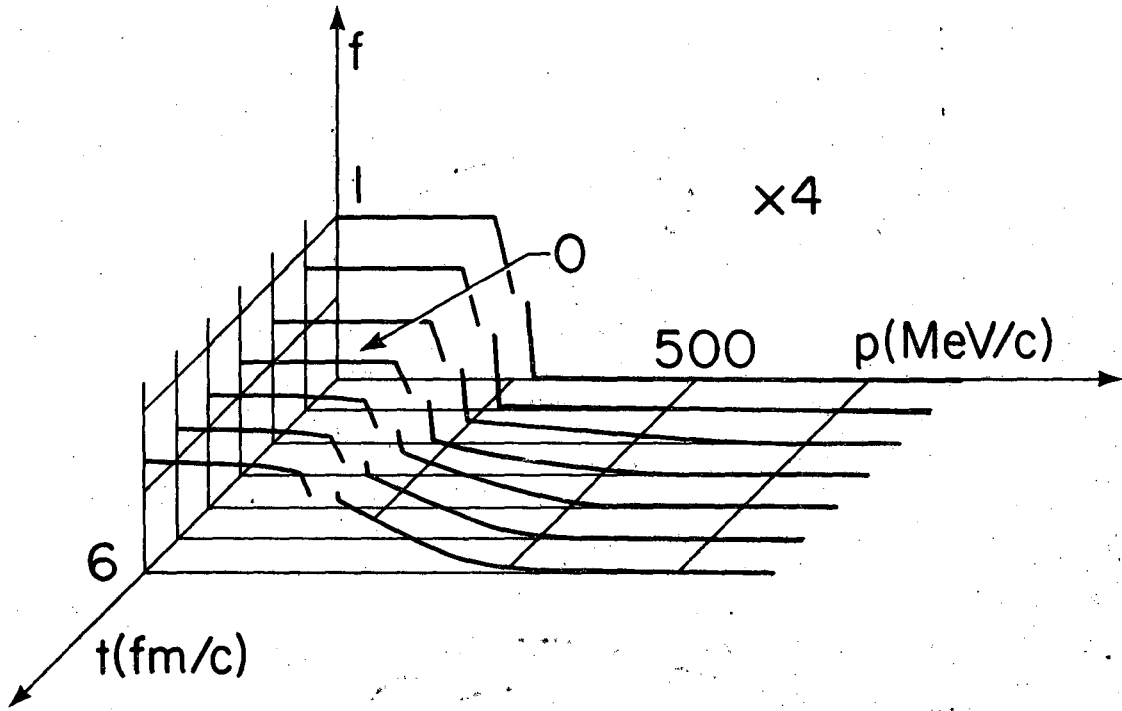
Fig. 2



XBL 829-11826

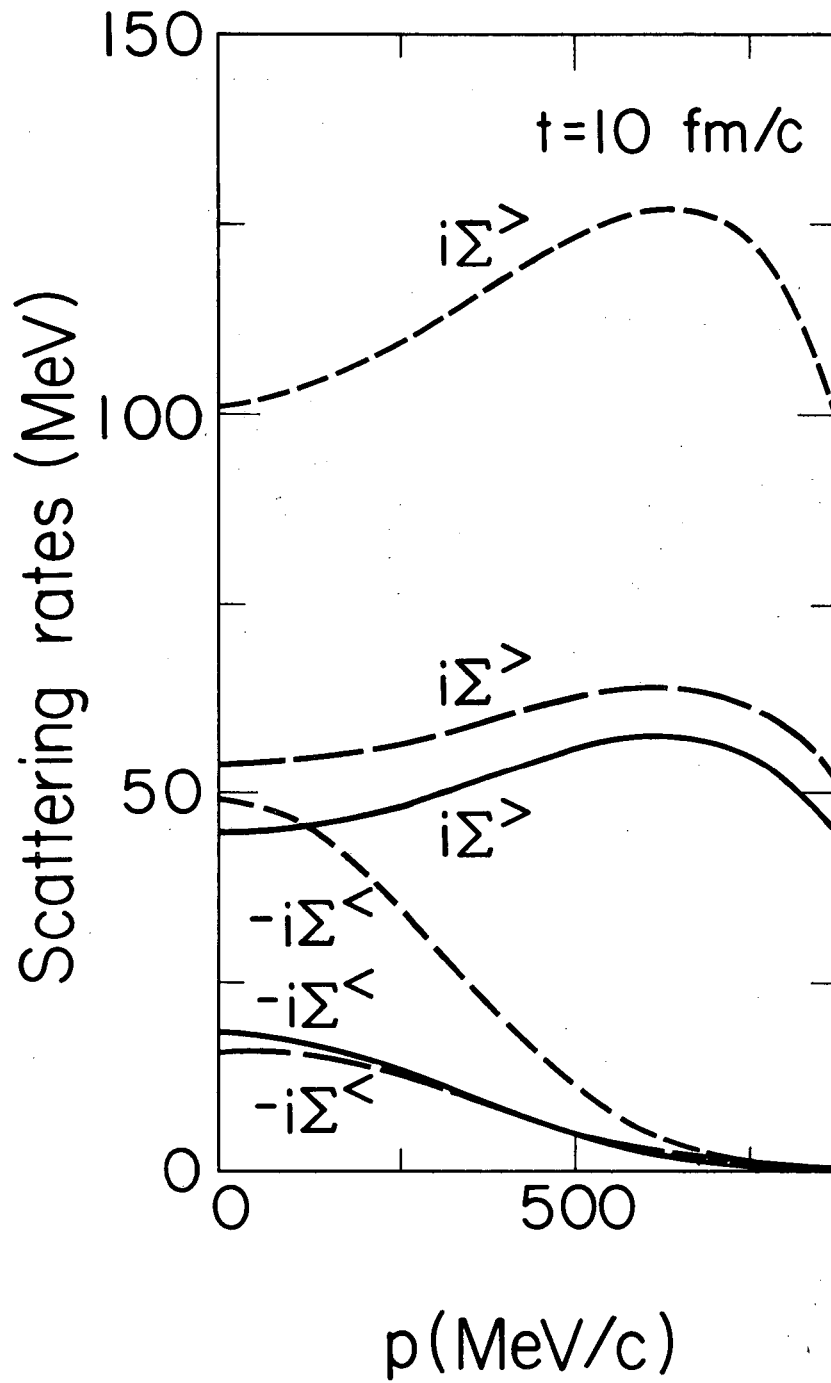
Fig. 3





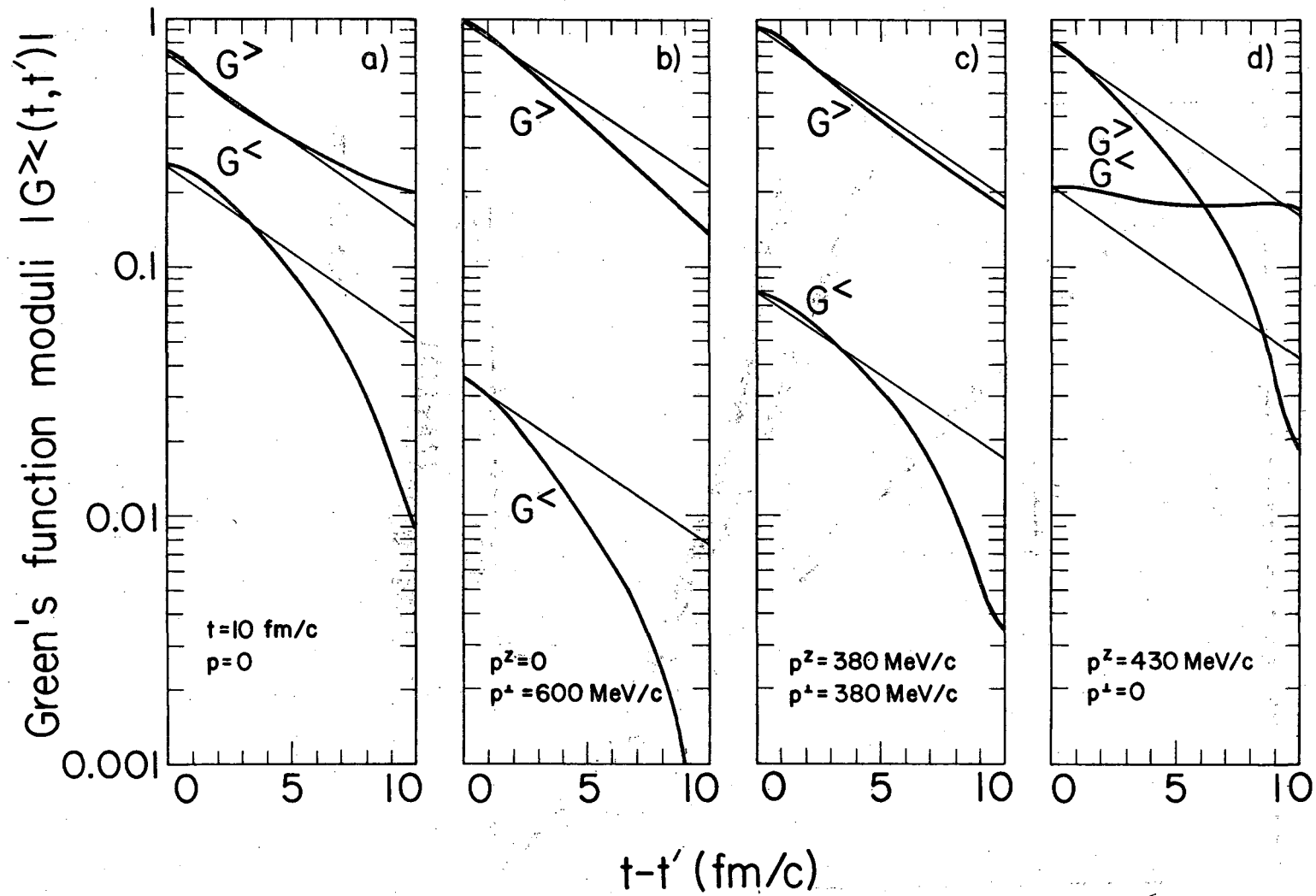
XBL829-4642

Fig. 4



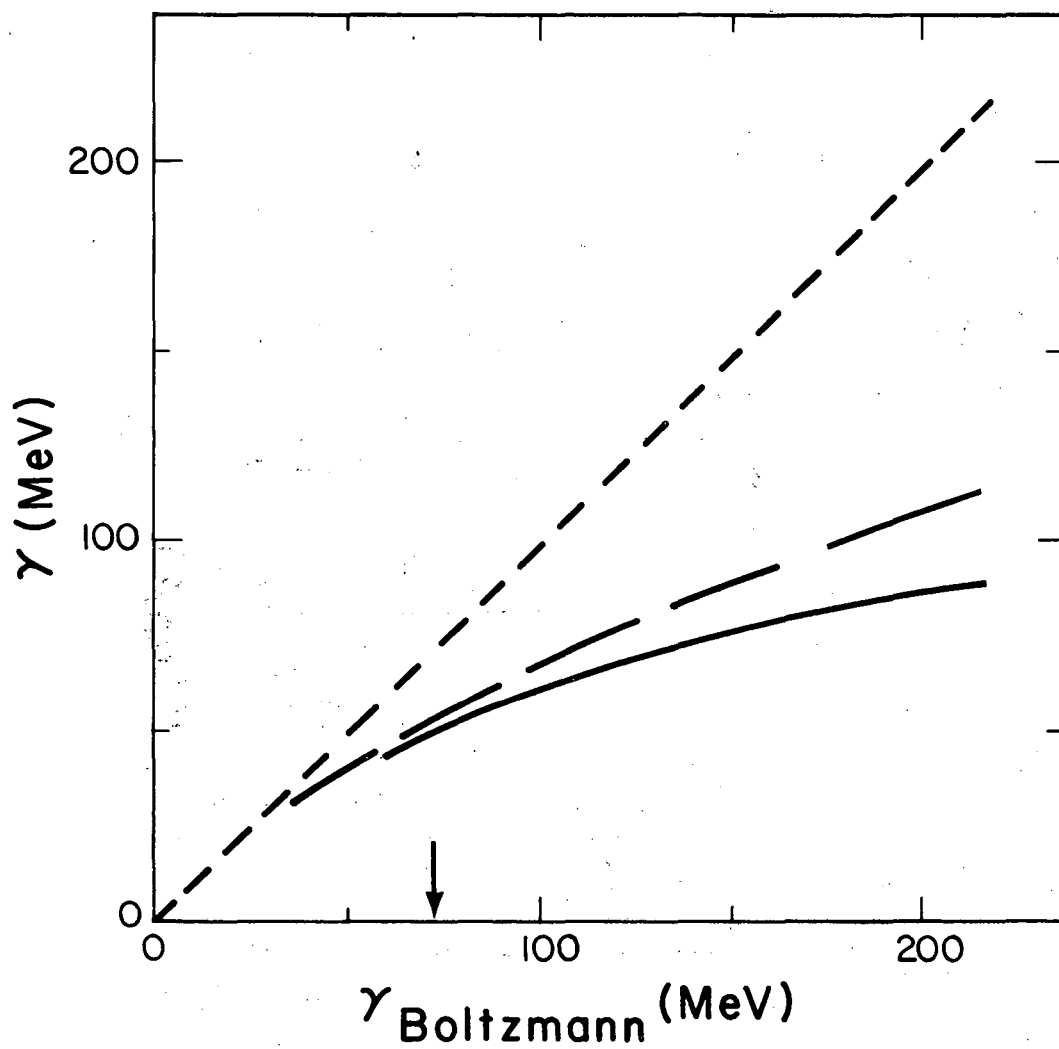
XBL829-4641

Fig. 5



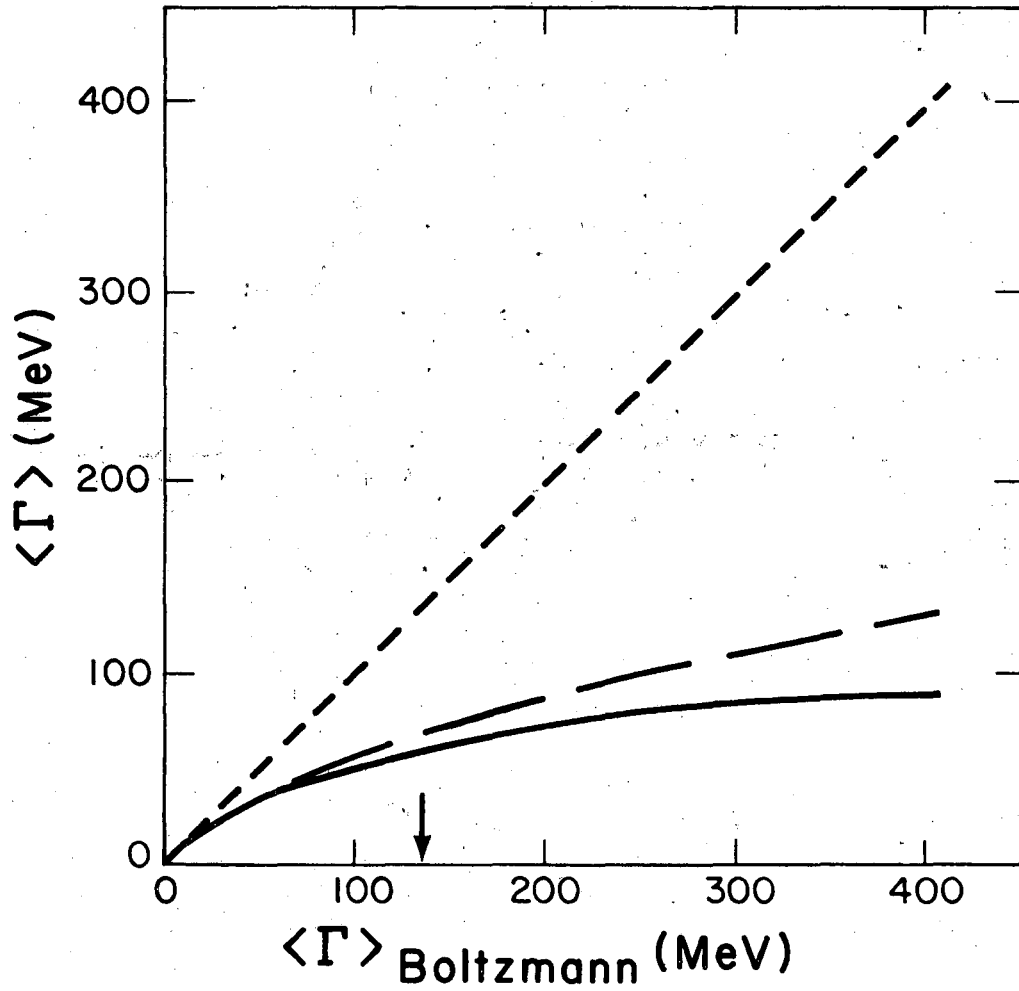
XBL829-4643

Fig. 6



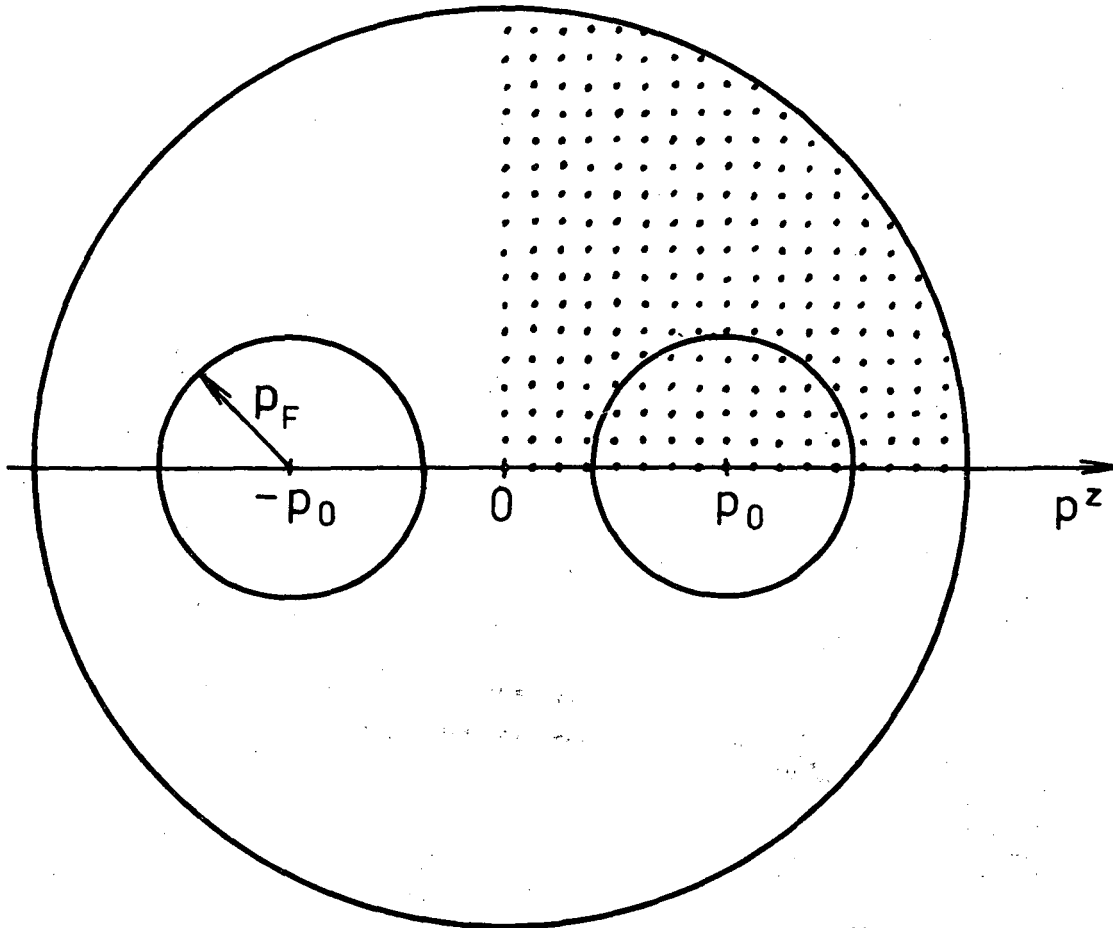
XBL 8210-4839

Fig. 7



XBL 8210-4840

Fig. 8



XBL 8211-3425

Fig. 9

This report was done with support from the Department of Energy. Any conclusions or opinions expressed in this report represent solely those of the author(s) and not necessarily those of The Regents of the University of California, the Lawrence Berkeley Laboratory or the Department of Energy.

Reference to a company or product name does not imply approval or recommendation of the product by the University of California or the U.S. Department of Energy to the exclusion of others that may be suitable.

TECHNICAL INFORMATION DEPARTMENT  
LAWRENCE BERKELEY LABORATORY  
UNIVERSITY OF CALIFORNIA  
BERKELEY, CALIFORNIA 94720